



Article

Identification of Vinyl Sulfone Derivatives as EGFR Tyrosine Kinase Inhibitor: In Vitro and In Silico Studies

Thitinan Aiebchun ¹, Panupong Mahalapbutr ², Atima Auepattanapong ³, Onnicha Khaikate ³, Supaphorn Seetaha ⁴, Lueacha Tabtimmai ⁵, Chutima Kuhakarn ³, Kiattawee Choowongkomon ^{4,*}, and Thanyada Rungrotmongkol ^{1,6,*}

- ¹ Biocatalyst and Environmental Biotechnology Research Unit, Department of Biochemistry, Faculty of Science, Chulalongkorn University, Bangkok 10330, Thailand; thitinan1906@gmail.com
- ² Department of Biochemistry, Faculty of Medicine, Khon Kaen University, Khon Kaen 40002, Thailand; panupma@kku.ac.th
- ³ Department of Chemistry and Center of Excellence for Innovation in Chemistry (PERCH-CIC), Faculty of Science, Mahidol University, Bangkok 10700, Thailand; iceatima.12@gmail.com (A.A.); onnicha.khai@gmail.com (O.K.); chutima.kon@mahidol.ac.th (C.K.)
- ⁴ Department of Biochemistry, Faculty of Science, Kasetsart University, Chatuchak, Bangkok 10900, Thailand; supaporn.se@ku.th
- ⁵ Department of Biotechnology, Faculty of Applied Science, King Mongkut's University of Technology of North Bangkok, Bangkok 10800, Thailand; Lueacha.t@sci.kmutnb.ac.th
- ⁶ Program in Bioinformatics and Computational Biology, Faculty of Science, Chulalongkorn University, Bangkok 10330, Thailand
- * Correspondence: kiattawee.c@ku.th (K.C.); t.rungrotmongkol@gmail.com (T.R.); Tel.: +66-2218-5426 (T.R.); Fax: +66-2218-5418 (T.R.)



Citation: Aiebchun, T.; Mahalapbutr, P.; Auepattanapong, A.; Khaikate, O.; Seetaha, S.; Tabtimmai, L.; Kuhakarn, C.; Choowongkomon, K.; Rungrotmongkol, T. Identification of Vinyl Sulfone Derivatives as EGFR Tyrosine Kinase Inhibitor: In Vitro and In Silico Studies. *Molecules* **2021**, *26*, 2211. <https://doi.org/10.3390/molecules26082211>

Academic Editor: Pascal Marchand

Received: 21 November 2020

Accepted: 7 April 2021

Published: 12 April 2021

Publisher's Note: MDPI stays neutral with regard to jurisdictional claims in published maps and institutional affiliations.



Copyright: © 2021 by the authors. Licensee MDPI, Basel, Switzerland. This article is an open access article distributed under the terms and conditions of the Creative Commons Attribution (CC BY) license (<https://creativecommons.org/licenses/by/4.0/>).

Abstract: Epidermal growth factor receptor (EGFR), overexpressed in many types of cancer, has been proved as a high potential target for targeted cancer therapy due to its role in regulating proliferation and survival of cancer cells. In the present study, a series of designed vinyl sulfone derivatives was screened against EGFR tyrosine kinase (EGFR-TK) using in silico and in vitro studies. The molecular docking results suggested that, among 78 vinyl sulfones, there were eight compounds that could interact well with the EGFR-TK at the ATP-binding site. Afterwards, these screened compounds were tested for the inhibitory activity towards EGFR-TK using ADP-Glo™ kinase assay, and we found that only VF16 compound exhibited promising inhibitory activity against EGFR-TK with the IC₅₀ value of 7.85 ± 0.88 nM. In addition, VF16 showed a high cytotoxicity with IC₅₀ values of 33.52 ± 2.57, 54.63 ± 0.09, and 30.38 ± 1.37 μM against the A431, A549, and H1975 cancer cell lines, respectively. From 500-ns MD simulation, the structural stability of VF16 in complex with EGFR-TK was quite stable, suggesting that this compound could be a novel small molecule inhibitor targeting EGFR-TK.

Keywords: EGFR tyrosine kinase; vinyl sulfone derivatives; in silico study; kinase assay; cytotoxicity assay

1. Introduction

Cancer is a devastating disease characterized by uncontrolled growth and spread of abnormal cells and is the second leading cause of mortality worldwide [1]. Nowadays, there are many types of cancer treatment such as chemotherapy, radiation therapy and targeted therapy [2–4]. Targeted cancer therapy has become one of the highly effective for cancer treatment due to its specificity towards cancer cells [5]. The overexpression of epidermal growth factor receptor (EGFR) in cancer cells leads to abnormal signal transduction and is closely related to the occurrence of cancer. Therefore, it has become one of the most important protein targets for designing and developing kinase inhibitors that act on oncogenic EGFR [6].

EGFR, a member of the ErbB family of receptor tyrosine kinases, plays important role in cellular signaling pathways, e.g., mitogen-activated protein kinase (MAPK), phosphoinositide 3-kinase (PI3K)/Akt, and signal transducer and activator of transcription (STAT) pathways that regulate key functions such as proliferation, survival, differentiation, and apoptosis [7]. EGFR is composed of an extracellular receptor domain, a single hydrophobic transmembrane region and an intracellular domain, which includes a juxta membrane domain [8], a tyrosine kinase (TK) domain and a C-terminal tyrosine-rich region [9]. The activation of EGFR-mediated signaling pathways begins with EGF binding to the extracellular domain, which activates the TK domain to phosphorylate at its C-terminal tail, and ultimately, initiates downstream signaling pathways [10,11]. Accordingly, targeting EGFR protein has been suggested as a promising strategy for targeted cancer therapy, since the EGFR is commonly overexpressed in many human cancers, including non-small cell lung, head, breast, bladder and ovarian carcinoma [12,13]. Consequently, inhibition of EGFR leads to the inhibition of cancer cells.

The clinically available drugs used as a tyrosine kinase inhibitor of EGFR (EGFR-TKI) such as erlotinib [14] and gefitinib [15]. The erlotinib is widely used in cancer patients for its inhibitory activity against EGFR exon 19 deletions or the L858R mutation [16,17]. However, these drugs have several side effects such as anemia, balance impairment, dizziness and headache. In addition, acquired drug resistance caused by the secondary mutation T790M of EGFR-TK domain develops inevitably after a median response duration of 9 to 13 months [18]. Therefore, the searching for promising compounds effectively targeting mutated EGFR-TK has become an imperative necessity [19,20].

Vinyl sulfone (VF) is an organic compound, where its core structure is similar to that of chalcones [21–24] (Figure 1). Previous study has shown that chalcone derivatives can inhibit EGFR activity with the IC_{50} value ranged from 10.3–15.4 μ M [25]. Thus, we hypothesized that VF derivatives can inhibit EGFR-TK activity in a manner similar to chalcones. In this study, we aimed to find new potential anti-cancer agents against EGFR-TK. A series of designed VF derivatives was initially screened by molecular docking technique. Subsequently, the kinase inhibition assay of the screened compounds against EGFR-TK was studied. Then, the *in vitro* cytotoxicity assay towards EGFR expressing lung carcinoma cell lines (A549 and A431) and T790M expressing lung cancer cell line (H1975) was conducted using MTT assay. Finally, the molecular dynamics simulation and free energy calculation were performed to investigate the structural and dynamics properties as well as the binding efficiency of the most potent VF in complex with EGFR-TK.

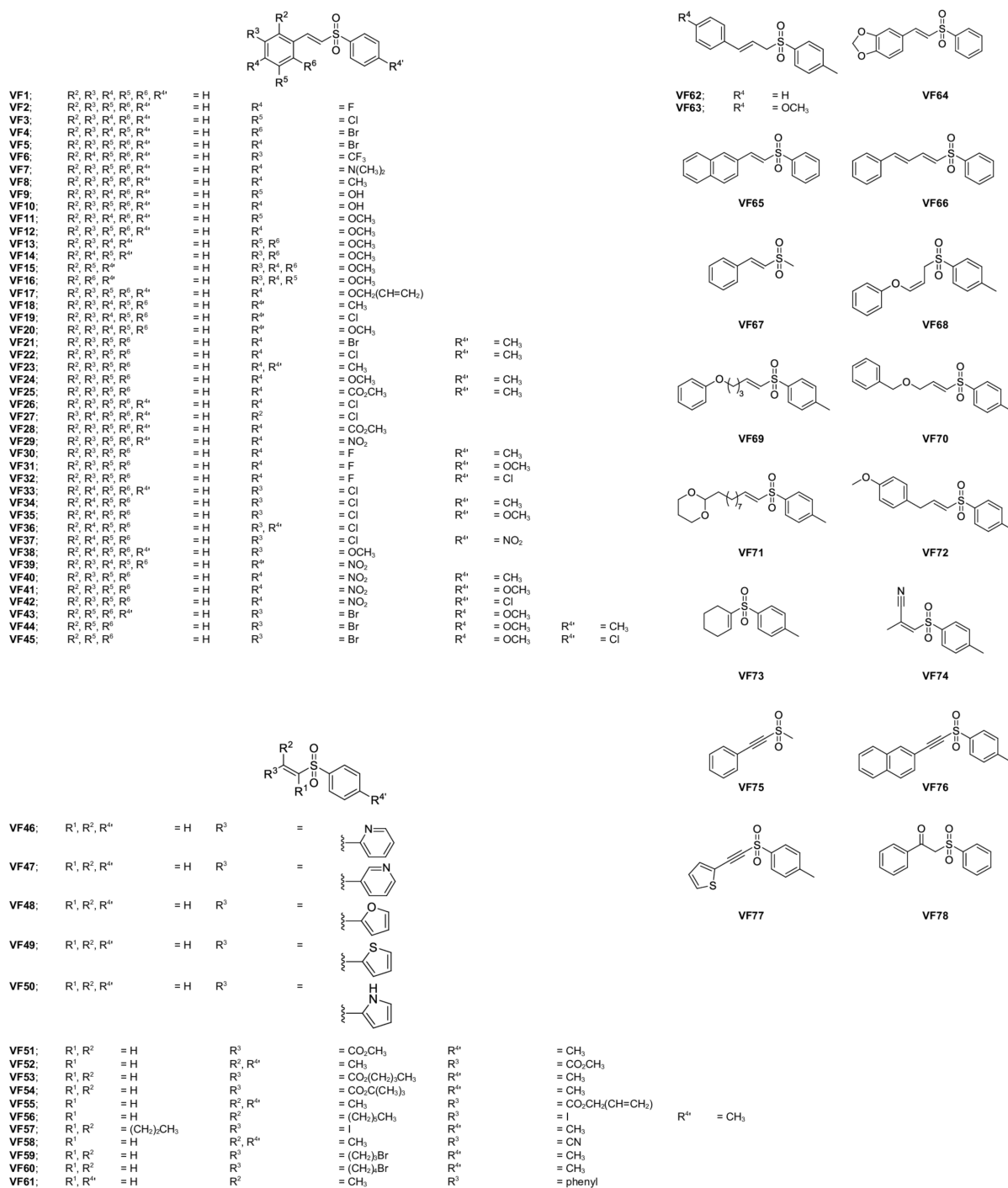


Figure 1. The chemical structures of VFs obtained from the previous study [21–24].

2. Results and Discussion

2.1. Molecular Docking

Initially, the 78 VFs (Figure 1) were investigated their binding mechanism using the CDocker module of Accelry Discovery Studio 3.0. Each compound was separately docked into the ATP-binding pocket of EGFR-TK complex. The interaction energy of erlotinib is -45.49 kcal/mol, while the interaction energy of all studied compounds is ranged from -43.47 to -21.61 kcal/mol. These results suggested that none of the vinyl sulfone derivatives is stronger than erlotinib. So, we cut off the compounds using the interaction energy lower than -37.5 kcal/mol, and we found eight VFs (VF15, VF16,

VF29, VF37, VF41, VF52, VF69 and VF71) that showed lower interaction energies than the others (Figure 2). These compounds can interact with important surrounding residues in ATP-binding pocket of EGFR-TK via H-bonding, pi interactions and van der Waals (vdW) forces (Figure 3). Interestingly, the sulfonate group of most compounds exhibited H-bond formation at the hinge region residue M769 (Figure 3A–I) [26,27] similar to erlotinib. The VF29, VF37, and VF41, which have nitro group as substituents, formed H-bond with T830 residue at A loop. Moreover, the matched vdW contacts between all VFs and erlotinib were as follows: (i) hinge region: T766, L768, P770, and G772 and (ii) A loop: K721, E731, T830, and D831. These results suggested that these eight VFs might be the potent candidate compounds acting against EGFR-TK.

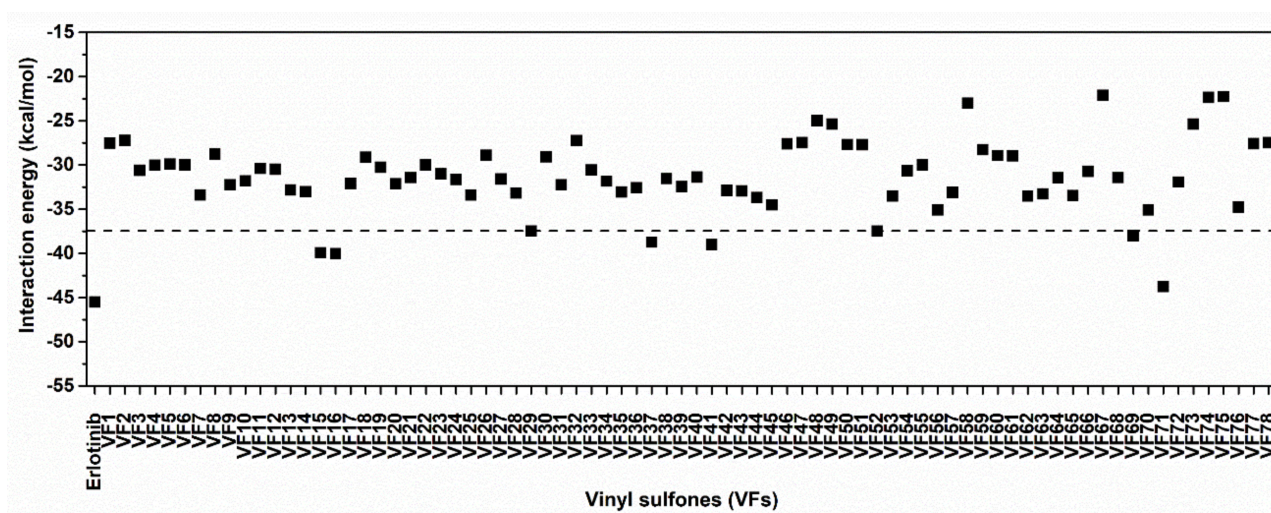


Figure 2. CDOCKER interaction energies of VFs and known drug erlotinib against EGFR-TK at ATP-binding site.

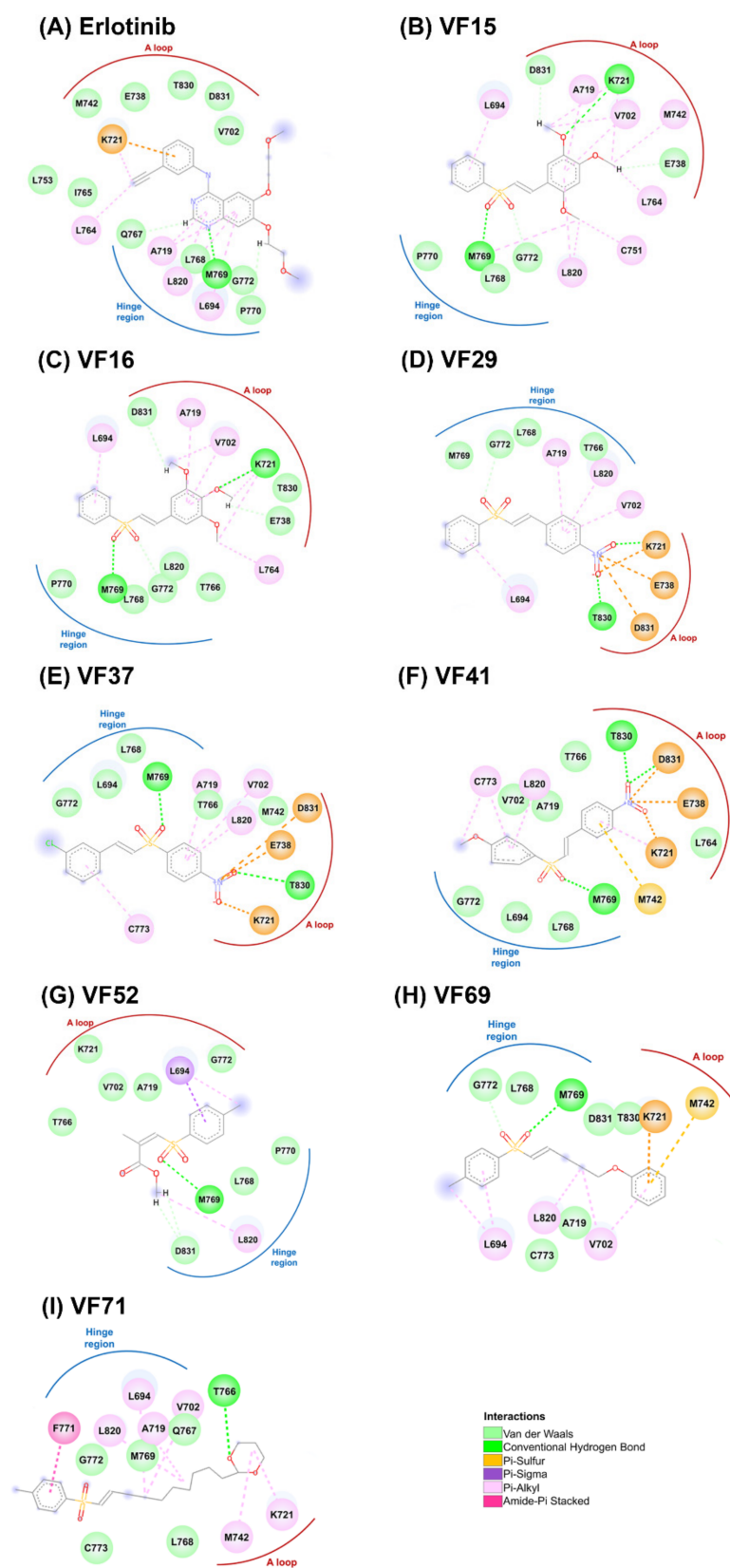


Figure 3. 2D interactions of EGFR-TK in complex with erlotinib (A) and VFs (B–I).

2.2. Drug-Likeness Prediction

Physical properties of the eight potent VFs were investigated in term of the drug-likeness by considering their physicochemical properties, including molecular weight (MW), the numbers of hydrogen bond donors (HBD) and acceptors (HBA), rotatable bond (RB), polar surface area (PSA) and lipophilicity (LogP) using the SwissADME web server [26]. The obtained results (Table 1) revealed that all VFs showed the acceptable value following the criteria: (i) $M_w \leq 500$ Da, (ii) $HBD \leq 5$ and $HBA \leq 10$, (iii) $RB \leq 10$, (iv) $PSA \leq 140$ Å, and (v) $LogP \leq 5$ [27]. Therefore, these VFs could likely be developed as promising novel EGFR-TK inhibitors.

Table 1. Predicted Lipinski's rule of five for the vinyl sulfones and the known drug. HBD, hydrogen bond donor; HBA, hydrogen bond acceptor; PSA, polar surface area.

| Compound | Lipinski's Rule of Five | | | | | | Drug-Likeness |
|------------------|-------------------------|---------------------|----------------------|---------------------|------------------------|----------------------|---------------|
| | MW (≤ 500 Da) | HBD (≤ 5) | HBA (≤ 10) | RB (≤ 10) | PSA (≤ 140 Å) | LogP (≤ 5) | |
| Erlotinib | 393.44 | 1 | 6 | 10 | 74.73 | 3.20 | Yes |
| VF15 | 334.39 | 0 | 5 | 6 | 70.21 | 2.76 | Yes |
| VF16 | 334.39 | 0 | 5 | 6 | 70.21 | 3.00 | Yes |
| VF29 | 291.32 | 2 | 4 | 4 | 86.22 | 2.32 | Yes |
| VF37 | 325.77 | 2 | 4 | 4 | 86.22 | 2.32 | Yes |
| VF41 | 321.35 | 2 | 5 | 5 | 95.45 | 2.66 | Yes |
| VF52 | 254.30 | 0 | 4 | 4 | 68.82 | 2.38 | Yes |
| VF69 | 316.41 | 0 | 3 | 7 | 51.75 | 3.26 | Yes |
| VF71 | 380.54 | 0 | 4 | 10 | 60.98 | 4.34 | Yes |

2.3. Inhibition of the EGFR-TK by Vinyl Sulfone Derivatives

Since the data shown above suggested that the eight VFs may be effective against EGFR-TK, we then investigated the EGFR-TKI inhibitory activity of the eight potent VFs and erlotinib at 1 μ M using ADP-Glo kinase assay (Figure 4A). Interestingly, we found that VF16 showed the highest EGFR-TK inhibitory activity (98.91%), which was higher than erlotinib (87.80%). Then, VF16 was selected to evaluate the half-maximal inhibitory concentration (IC_{50}) values. As shown in Figure 4B, the IC_{50} against EGFR-TK of VF16 is 7.85 ± 0.88 nM, which is significantly lower than the erlotinib (IC_{50} of 26.09 ± 5.42 nM). Additionally, the inhibitory activity of VF16 is greater than that of the chalcones that have been previously reported to inhibit EGFR activity (IC_{50} ranked from 10.3 to 15.4 μ M) [25].

In order to confirm the inhibition selectivity of VF16 towards EGFR-TK, we further performed kinase inhibition assay of VF16 against JAK3 and HER2 protein kinases because both kinases are one of the most studied kinase families [28,29]. The obtained results showed that VF16 showed very low inhibitory activity against JAK3 (IC_{50} of 158.45 ± 4.75 nM) and HER2 (IC_{50} of 312.00 ± 0.28 nM) (Figure S3) as compared to EGFR-TK (IC_{50} of 7.85 ± 0.88 nM), suggesting that VF16 was specific to EGFR-TK rather than JAK3 and HER2.

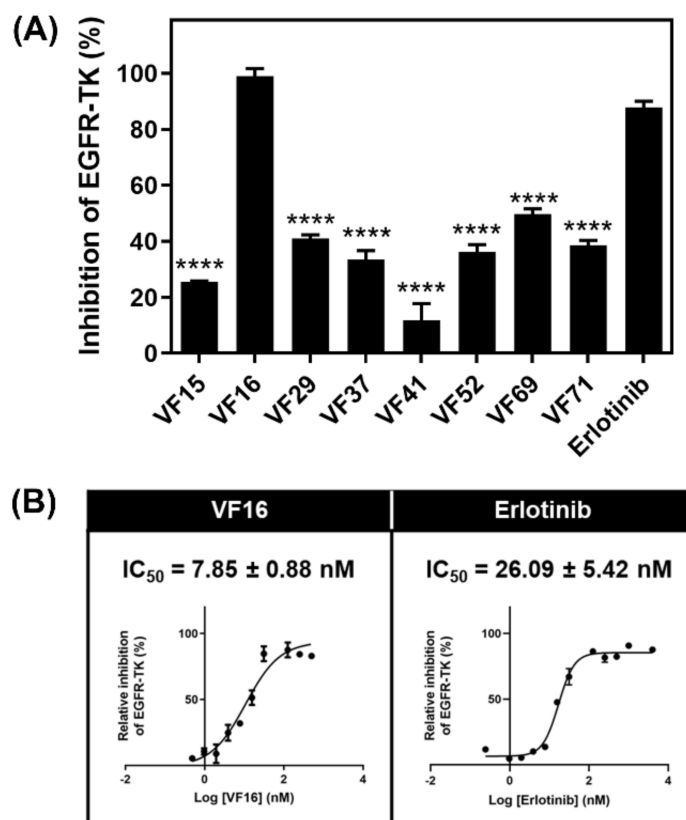


Figure 4. (A) Kinase inhibitory activity screening of VFs towards EGFR-TK at 1 μ M. **** $p \leq 0.0001$ vs. erlotinib. (B) Kinase inhibitory activity of VFs towards EGFR-TK. Data are represented as means \pm SEM from triplicate independent experiments.

2.4. Cytotoxicity

The VF16 was selected to evaluate IC₅₀ values against A549 and A431 cell lines overexpressing wild-type EGFR (A549 and A431) and mutant EGFR human lung cancer cell line (H1975) using MTT assay. The obtained results (Figure 5) revealed that the cytotoxic activity of VF16 against A549 (IC₅₀ of 54.63 \pm 0.09 μ M) and A431 (IC₅₀ of 33.52 \pm 2.57) was similar to that of erlotinib (IC₅₀ of 48.21 \pm 7.43 μ M and 27.19 \pm 6.93 μ M for A549 and A431, respectively). Note that VF16 inhibited the A431 cells better than A549 cells because (i) the EGFR expression level found in A431 cells is dramatically higher than that found in A549 [30] and (ii) A549 cells exhibits KRAS mutation, which constitutively activates downstream MAPK signaling pathways, causing a compensatory mechanism [31]. In H1975 cells, the VF16 (IC₅₀ of 30.38 \pm 1.37 μ M) was more susceptible than the erlotinib (IC₅₀ of 98.93 \pm 1.74 μ M) by \sim 3 times. The lower susceptibility of erlotinib towards T790M EGFR-expressing cells (H1975) compared to wild-type EGFR-expressing cells (A549 and A431) is in good agreement with the previous studies [32–34]. Altogether, these findings suggested that VF16 exhibited potent anti-lung cancer activity in all three lung cancer cell lines, which could be developed as a novel anti-lung cancer agent.

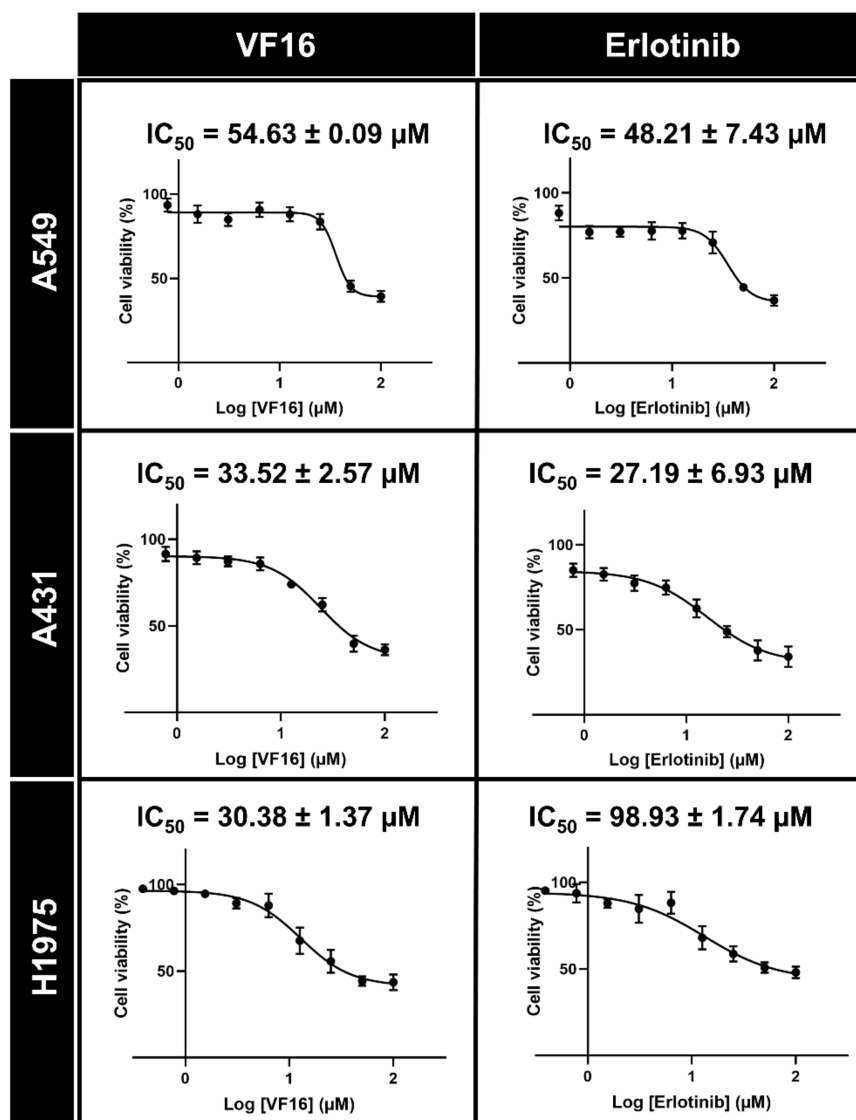


Figure 5. Cytotoxicity in three cancer cell lines (A549, A431, and H1975) after treated with various concentrations of VF16 compared to the known drug erlotinib for 72 h. Data are represented as means \pm SEM from triplicate independent experiments.

2.5. Molecular Dynamics Simulation

The structural stability of VF16 bound to the EGFR-TK domain was characterized using RMSD calculation plotted along the simulation time, and the obtained results are illustrated in Figure 6A. The RMSD values of VF16 were slightly fluctuated at the first 150 ns and then reached the equilibrium state after 250 ns with an average RMSD value of $\sim 0.5\text{--}2 \text{ \AA}$. In the case of whole protein and backbone of protein, the RMSD values were slightly fluctuated at the first 100 ns then showed the stable values along the last stage of MD simulation with an average RMSD value of $\sim 2\text{--}3.5 \text{ \AA}$.

In addition, the MD trajectories of this system were selected for further analysis in terms of: (i) the number of H-bond and (ii) number of contact atom within the 3.5 \AA sphere of VF16, respectively. The number of intermolecular hydrogen bonds and intermolecular contacts between VF16 and its surrounding residues was computed along 500 ns MD simulation represented in Figure 6A. According to the results, we found that VF16 formed two H-bonds with the M769 and C797, in which the C797 could form stronger H-bond than the M769. In addition, we found ~ 10 intermolecular contacts steadily formed between VF16 and EGFR-TK. These findings suggested that our simulation model was stable. In this

work, the MD trajectories from 300 to 500 ns were thus extracted for further analysis in terms of ΔG_{bind} values (kcal/mol) and key binding residues of VF16 against EGFR-TK.

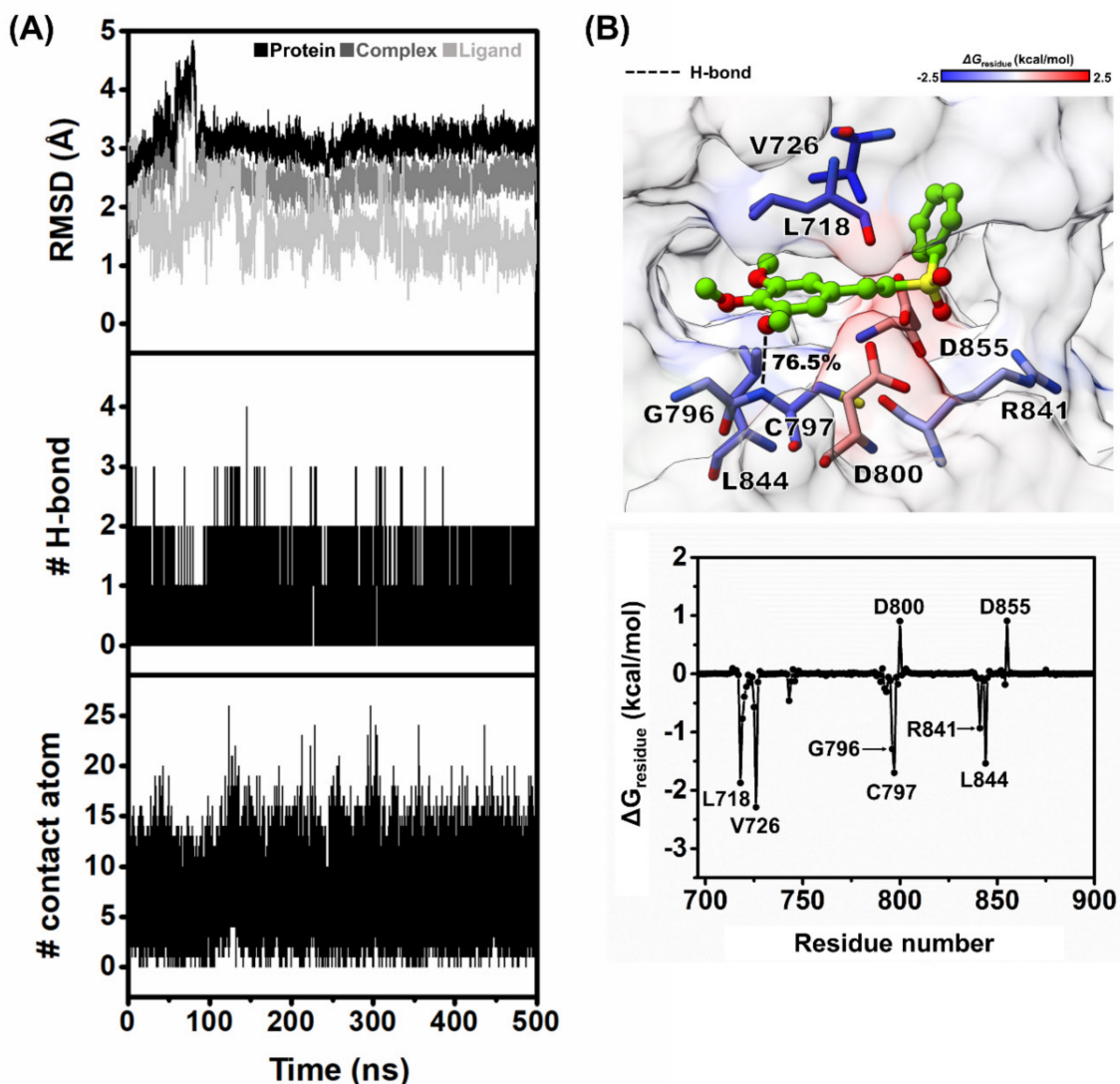


Figure 6. (A) All-atom RMSD, number of H-bonds, and number of contacts atom of VF16 in complex with EGFR-TK plotted along the 500 ns MD simulation. (B) Binding orientation of VF16 inside the ATP-binding pocket of EGFR-TK. The contributing residues involved in ligand binding are colored according to their $\Delta G_{\text{residue}}$ values, where the highest to lowest free energies are shaded from blue to red, respectively (H-bond interaction represented by black dash line) and per-residue decomposition free energy of the VF16 complex with EGFR-TK.

2.6. Binding Affinity and Key Residues for VF16/EGFR-TK Complex

The free energy calculation based on MM-GBSA method was applied to predict the binding affinity of VF16/EGFR-TK complex. We found that the ΔG_{bind} of VF16 is almost identical to the ΔG_{Exp} (Table 2). To investigate the key residues of EGFR-TK for VF16 binding, the per-residue decomposition free energy ($\Delta G_{\text{residue}}$) based on the MM-GBSA method was applied on the 100 snapshots over the last 200 ns MD simulation. Note that among residues 695–1018, only residues 695–900 are shown in Figure 6B, where the binding orientation of VF16 inside the ATP-binding pocket of EGFR-TK is shown in Figure 6B. The obtained results revealed that there were eight residues (L718, V726, G796, C797, D800, R841, L844, and D855) that were important for the binding of VF16. The binding residues of VF16 observed in this work were also found as a major interaction in erlotinib/EGFR-TK

complex (including L718, A743, L792, M793, G796, and L844) [35,36]. Figure 6B showed binding orientation inside the ATP-binding pocket of VF16/EGFR-TK complex, and we found that the $-OCH_3$ moiety of VF16 strongly formed H-bond with C797 and weakly formed H-bond with M769. This is in good agreement with the previous reports showing that H-bond formation with M769 is the main interaction of erlotinib and gefitinib in complex with wild-type EGFR and mutant EGFR [37–40].

Table 2. The MM-GBSA ΔG_{bind} and its energy components (kcal/mol).

| Energy Component | ΔG_{bind} (kcal/mol) |
|---------------------------|-------------------------------------|
| ΔE_{vdW} | -38.99 ± 0.29 |
| ΔE_{ele} | -12.95 ± 0.55 |
| ΔG_{gas} | -51.94 ± 0.68 |
| ΔG_{solv} | 24.69 ± 0.53 |
| ΔG_{bind} | -8.74 ± 0.32 |
| ΔG_{Exp}^a | -10.13 ± 0.88 |

^a Experimental binding free energies (ΔG_{Exp}) was converted from the IC_{50} value using the Cheng-Prusoff equation of $\Delta G_{\text{Exp}} = RT \ln(IC_{50})$ [41].

3. Materials and Methods

3.1. Interaction Energies between Vinyl Sulfone Derivatives and the ATP-Binding Site of EGFR-TK by Molecular Docking Technique

The crystal structure of EGFR complexed with erlotinib (PDB ID: 1M17) [39] was downloaded from Protein Data Bank (PDB). The 3D structure of the drug (erlotinib) was obtained from the ZINC database, whilst the 3D structures of vinyl sulfone derivatives were generated using the Gaussian 09 program. Note that the vinyl sulfone derivatives were constructed according to their availability from previous study [21–24]. All the ligands were optimized using the Gaussian 09 program (HF/6–31d) as per the standard protocol [42–44]. The protonation state of all studied ligands was characterized using the ChemAxon [45].

For system validation, the crystalized ligands were defined as a center in the active site for redocking using CDOCKER programs and the results are shown in Supplementary Figure S1. The docking protocols of EGFR system was set as 15 Å for sphere docking and docked into the binding pocket with 100 independent runs. The binding between protein and compounds/drug was visualized using the Accelrys Discovery Studio 3.0 (Accelrys Inc., Cambridge, UK) and UCSF Chimera package [46].

3.2. Predicted Physicochemical Properties

Physicochemical features such as hydrogen bond donors, hydrogen bond acceptors and drug-likeness play an important role in drug discovery and development [47]. Herein, such properties of the potent compounds were calculated in comparison with known drugs (erlotinib) using web-based applications SwissADME (www.swissadme.ch/) (accessed on 19 June 2020) [26].

3.3. Chemical Reagents and Cell Lines

The ADP-Glo™ Kinase Assay kit was purchased from Promega (Madison, WI, USA). EGFR and HER2 was obtained from the previous report [48]. JAK3 (SRP0173) were purchased from Sigma-Aldrich (Darmstadt, Germany). The series of vinyl sulfone derivatives were kindly provided by Dr. Chutima Kuhakarn from Department of Chemistry and Center of Excellence for Innovation in Chemistry (PERCH-CIC), Faculty of Science, Mahidol University [21–24]. Note that, due to limited amounts of vinyl sulfones obtained from previous study, we performed EGFR kinase and cytotoxicity assays as well as binding pattern study at the molecular level on only 78 vinyl sulfone derivatives (Figure 1). The lung carcinoma A549 (ATCC CCL-185) and A431 (ATCC CRL-1555) cell lines were purchased from the American Type Cell Culture Collection (ATCC,

Manassas, VA, USA). The EGFR mutated human lung cancer cell line (H1975) was provided by Dr. Chanida Vinayanuwattikun from Department of Medicine, Chulalongkorn University. Dulbecco's modified Eagle's medium (DMEM), RPMI-1640 medium, fetal bovine serum (FBS), penicillin-streptomycin (Pen-Strep) and trypsin were purchased from Life Technologies (California, USA). 3-(4,5-dimethylthiazol-2-yl)-2,5-diphenyltetrazolium bromide (MTT) and dimethyl sulfoxide (DMSO) were purchased from Sigma-Aldrich (Darmstadt, Germany).

3.4. Inhibition of the EGFR-TK by Vinyl Sulfone Derivatives

The selected sulfone derivatives that had the interaction energy lower or equal than erlotinib and physicochemical properties showed the acceptable value, were screened for their ability to inhibit the tyrosine kinase activity of the EGFR using the ADP-GloTM kinase assay as previously reported [25,49]. The first 8 μ L of buffer (40 mM Tris-HCl pH 7.5, 20 mM MgCl₂, and 0.1 mg/mL bovine serum albumin) was added to a 384-well plate. Then, 5 μ L of EGFR enzymes (1.25 ng/ μ L) and 2 μ L of inhibitors were added, followed by 10 μ L of a mixture of 5 μ M ATP and 2.5 μ M poly(glu-tyr), and incubated for 1 h at room temperature. Next, 5 μ L of the ADP-Glo reagent was added and incubated for 40 min, after that, 10 μ L of kinase detection reagent was added and incubated at room temperature for 30 min to convert the ADP to ATP. The ATP was then detected by measuring the luminescence using a microplate reader (Infinite M200 microplate reader, Tecan, Männedorf, Switzerland). All assays were performed in triplicate. The relative inhibition (%) of inhibitors were then calculated compared to the control with no inhibitor as shown in Equation (1):

$$\% \text{Relative inhibition} = \frac{[(\text{positive} - \text{negative}) - (\text{sample} - \text{negative})]}{(\text{positive} - \text{negative})} \times 100 \quad (1)$$

From this equation, the positive is the addition of the enzyme in the reaction, while the negative is without the enzyme in the reaction.

3.5. Cell Cultures

The A549 and A431 cells were grown in complete DMEM medium supplemented with 10% (*v/v*) FBS, 100 U/mL penicillin and 100 μ g/mL streptomycin. All cells were maintained at 37 °C in a 5% (*v/v*) CO₂, 95% (*v/v*) air humidified incubator while H1975 cells was grown in complete RPMI-1640 medium at 37 °C in a 5% (*v/v*) CO₂, 95% (*v/v*) air humidified incubator.

3.6. Cytotoxicity in Cancer Cell Lines

The in vitro cytotoxicity activity of vinyl sulfone derivatives against the A549, A431 and H1975 cell lines were evaluated using the MTT assay. The first 100 μ L of A549 (5000 cells/well), A431 (5000 cells/well) and H1975 (5000 cells/well) cells suspension was seeded per well in a 96-well microplate and incubated at 37 °C overnight, cells were treated with compounds and known drug (erlotinib) different concentration. Then, incubated for 72 h. Subsequently, the MTT solution (5 mg/mL) was added in A549, A431 and H1975 cells and incubated at 37 °C for 3 h. The medium was removed and 50 μ L of DMSO was added to each well to lyse the cells. Finally, the absorbance was measured at 570 nm using a microplate reader (Infinite M200 microplate reader, Tecan, Männedorf, Switzerland).

3.7. Molecular Dynamics Simulation

The starting crystal structure of EGFR-TK (PDB ID: 1M17) [39] was obtained from Protein Data Bank (PDB). The 3D structure of vinyl sulfone derivatives and known drug inhibitor (EGFR-TK) of EGFR-TK were generated and optimized HF/6-31G(d) method implemented in the Gaussian09 software [42–44]. The protein-ligand complexes were generated using the CDocker module accordance the standard protocol [50]. The docked VFs/EGFR-TK complex with lowest interaction energy and binding pattern similar to

the erlotinib (Figure S2) was selected as the initial structure for performing the Molecular Dynamics Simulation studies. The electrostatic potential (ESP) charges were consequently calculated with the same level of theory and were then fitted into restrained ESP (RESP) charges using the ANTECHAMBER module of AMBER16 [44,51,52]. The FF14SB [53] and GAFF [42,54] force fields were applied for protein and VF16, respectively. All missing hydrogen atoms of protein and ligand were added using LEaP module and were then minimized in order to remove the bad contacts. Each system was neutralized by the counter ions and immersed in a TIP3P water [55] box that extended at least 13 Å from the protein surface. Afterward, the complexes were energy-minimized by 1500 interactions of steepest descent (SD) and conjugated gradient (CG) methods using AMBER16 with the AMBER ff14SB force field.

The simulations are carried out under periodic boundary condition with NPT ensemble using a time step of 2 fs. The short-range cutoff for nonbonded interactions is set as 10 Å, whilst the Particle Mesh Ewald (PME) summation approach is applied to treat long-range electrostatic interaction [56,57]. Temperature and pressure are controlled by Berendsen weak coupling algorithm. The SHAKE algorithm is used to constrain all covalent bonds involving hydrogen atoms [58]. The simulated models are then heated up to 310 K for 100 ps and are continuously held at this temperature for another 100 ns or until the simulations have reached equilibrium. Finally, the structural and dynamics behaviors of each complex will be analyzed, including root mean square deviation (RMSD), number of H-bonds between the ligand and EGFR-TK and number of contact atom via the cptraj module [59]. Besides, the MM-GBSA and ΔG_{bind} , residue were calculated by the MM-PBSA.py module [58,59].

3.8. Statistical Analysis

The data are represented as mean \pm standard error of mean (SEM). Differences between groups were compared using one-way ANOVA, followed by Tukey's test for multiple comparisons. The differences in means were determined at the confidence level $p \leq 0.05$.

4. Conclusions

This work combined the computational and experiment techniques to identify new EGFR inhibitor based on vinyl sulfone derivatives. Eight vinyl sulfones from molecular docking technique were tested the inhibitory activity against EGFR-TK and cell-based assay in three cancer cell lines (A549, A431, and H1975 cell lines). The results showed that VF16 can inhibit EGFR-TK activity better than the approved drug erlotinib and showed higher cytotoxicity against A431 cell line than A549 cell line. Additionally, showed high cytotoxicity against H1975 cell lines. From MD simulations, our simulation model of VF16/EGFR are stable. In addition, VF16 showed strongest H-bond with C797, and the key residues responsible for VF16 binding were L718, V726, G796, C797, D800, R841, L844, and D855, in which these binding residues were also found in a major interaction between erlotinib and EGFR-TK. Thus, VF16 could be developed as a promising new anti-cancer drug targeting EGFR-TK.

Supplementary Materials: Figure S1: Superimposition of ligands between X-ray structure and CDocker docking, Figure S2: Binding pose between VF16 and known drug within EGFR-TK, Figure S3: The IC₅₀ curves of kinase inhibitory activity of VF16 against EGFR-TK, JAK3, and HER2.

Author Contributions: T.R., K.C., T.A., P.M. conceived and designed the experiments. T.A. conducted theoretical and experimental studies. A.A., O.K. and C.K. synthesized all compounds. T.A., P.M., T.R., K.C., L.T., and S.S. analyzed the data. T.A. wrote the original manuscript. All authors reviewed and edited the manuscript. All authors have read and agreed to the published version of the manuscript.

Funding: This work was financially supported by Ratchadaphiseksomphot Endowment Fund (Grant No. CU_GR_62_96_23_35 for T.R.). T.A. thanks the 90th Anniversary of Chulalongkorn University Fund (Rachadaphiseksomphot Endowment Fund, GCUGR1125633082M). C.K. thanks

the Thailand Research Fund (BRG6180005) and the Center of Excellence for Innovation in Chemistry, Ministry of Higher Education, Science, Research and Innovation.

Data Availability Statement: Data contained in the manuscript are available from the authors.

Acknowledgments: We would like to thank Siwaporn Boonyasuppayakorn, Department of Microbiology, Faculty of Medicine, Chulalongkorn University for supporting cell culture laboratory.

Conflicts of Interest: The authors declared no conflict of interest.

Sample Availability: Samples of the compounds are available from the authors.

References

1. Siegel, R.L.; Miller, K.D.; Jemal, A. Cancer statistics, 2019. *CA Cancer J. Clin.* **2019**, *69*, 7–34. [[CrossRef](#)] [[PubMed](#)]
2. Araujo, D.V.; Watson, G.A.; Oliva, M.; Heirali, A.; Coburn, B.; Spreafico, A.; Siu, L.L. Bugs as Drugs: The Role of Microbiome in Cancer Focusing on Immunotherapeutics. *Cancer Treat. Rev.* **2020**, *92*, 102125. [[CrossRef](#)] [[PubMed](#)]
3. Huang, M.; Shen, A.; Ding, J.; Geng, M. Molecularly targeted cancer therapy: Some lessons from the past decade. *Trends Pharmacol. Sci.* **2014**, *35*, 41–50. [[CrossRef](#)] [[PubMed](#)]
4. Sharma, S.V.; Settleman, J. Oncogene addiction: Setting the stage for molecularly targeted cancer therapy. *Genes Dev.* **2007**, *21*, 3214–3231. [[CrossRef](#)]
5. Ke, X.; Shen, L. Molecular targeted therapy of cancer: The progress and future prospect. *Front. Lab. Med.* **2017**, *1*, 69–75. [[CrossRef](#)]
6. Wee, P.; Wang, Z. Epidermal Growth Factor Receptor Cell Proliferation Signaling Pathways. *Cancers* **2017**, *9*, 52. [[CrossRef](#)]
7. Holbro, T.; Hynes, N.E. ErbB receptors: Directing key signaling networks throughout life. *Annu. Rev. Pharmacol. Toxicol.* **2004**, *44*, 195–217. [[CrossRef](#)]
8. Choowongkamon, K.; Carlin, C.R.; Sonnichsen, F.D. A structural model for the membrane-bound form of the juxtamembrane domain of the epidermal growth factor receptor. *J. Biol. Chem.* **2005**, *280*, 24043–24052. [[CrossRef](#)]
9. Flynn, J.F.; Wong, C.; Wu, J.M. Anti-EGFR Therapy: Mechanism and Advances in Clinical Efficacy in Breast Cancer. *J. Oncol.* **2009**, *2009*, 526963. [[CrossRef](#)]
10. Seshacharyulu, P.; Ponnusamy, M.P.; Haridas, D.; Jain, M.; Ganti, A.K.; Batra, S.K. Targeting the EGFR signaling pathway in cancer therapy. *Expert Opin. Ther. Targets* **2012**, *16*, 15–31. [[CrossRef](#)]
11. Fitzgerald, T.L.; Lertpiriyapong, K.; Cocco, L.; Martelli, A.M.; Libra, M.; Candido, S.; Montalto, G.; Cervello, M.; Steelman, L.; Abrams, S.L.; et al. Roles of EGFR and KRAS and their downstream signaling pathways in pancreatic cancer and pancreatic cancer stem cells. *Adv. Biol. Regul.* **2015**, *59*, 65–81. [[CrossRef](#)]
12. Ogiso, H.; Ishitani, R.; Nureki, O.; Fukai, S.; Yamanaka, M.; Kim, J.H.; Saito, K.; Sakamoto, A.; Inoue, M.; Shirouzu, M.; et al. Crystal structure of the complex of human epidermal growth factor and receptor extracellular domains. *Cell* **2002**, *110*, 775–787. [[CrossRef](#)]
13. Yang, C.H.; Chou, H.C.; Fu, Y.N.; Yeh, C.L.; Cheng, H.W.; Chang, I.C.; Liu, K.J.; Chang, G.C.; Tsai, T.F.; Tsai, S.F.; et al. EGFR over-expression in non-small cell lung cancers harboring EGFR mutations is associated with marked down-regulation of CD82. *Biochim. Biophys. Acta* **2015**, *1852*, 1540–1549. [[CrossRef](#)]
14. Wang, Y.; Schmid-Bindert, G.; Zhou, C. Erlotinib in the treatment of advanced non-small cell lung cancer: An update for clinicians. *Ther. Adv. Med. Oncol.* **2012**, *4*, 19–29. [[CrossRef](#)]
15. Maemondo, M.; Inoue, A.; Kobayashi, K.; Sugawara, S.; Oizumi, S.; Isobe, H.; Gemma, A.; Harada, M.; Yoshizawa, H.; Kinoshita, I.; et al. Gefitinib or Chemotherapy for Non-Small-Cell Lung Cancer with Mutated EGFR. *N. Engl. J. Med.* **2010**, *362*, 2380–2388. [[CrossRef](#)]
16. Liu, W.; Ning, J.F.; Meng, Q.W.; Hu, J.; Zhao, Y.B.; Liu, C.; Cai, L. Navigating into the binding pockets of the HER family protein kinases: Discovery of novel EGFR inhibitor as antitumor agent. *Drug Des. Devel. Ther.* **2015**, *9*, 3837–3851. [[CrossRef](#)]
17. Jackman, D.M.; Yeap, B.Y.; Sequist, L.V.; Lindeman, N.; Holmes, A.J.; Joshi, V.A.; Bell, D.W.; Huberman, M.S.; Halmos, B.; Rabin, M.S.; et al. Exon 19 deletion mutations of epidermal growth factor receptor are associated with prolonged survival in non-small cell lung cancer patients treated with gefitinib or erlotinib. *Clin. Cancer Res.* **2006**, *12*, 3908–3914. [[CrossRef](#)]
18. Cortot, A.B.; Janne, P.A. Molecular mechanisms of resistance in epidermal growth factor receptor-mutant lung adenocarcinomas. *Eur. Respir. Rev.* **2014**, *23*, 356–366. [[CrossRef](#)]
19. Tang, J.; Salama, R.; Gadgeel, S.M.; Sarkar, F.H.; Ahmad, A. Erlotinib resistance in lung cancer: Current progress and future perspectives. *Front. Pharmacol.* **2013**, *4*, 15. [[CrossRef](#)]
20. Politi, K.; Fan, P.D.; Shen, R.; Zakowski, M.; Varmus, H. Erlotinib resistance in mouse models of epidermal growth factor receptor-induced lung adenocarcinoma. *Dis. Model. Mech.* **2010**, *3*, 111–119. [[CrossRef](#)]
21. Katrun, P.; Hlekhilai, S.; Meesin, J.; Pohmakotr, M.; Reutrakul, V.; Jaipetch, T.; Soorukram, D.; Kuhakarn, C. PhI(OAc)₂ mediated decarboxylative sulfonylation of beta-aryl-alpha, beta-unsaturated carboxylic acids: A synthesis of (E)-vinyl sulfones. *Org. Biomol. Chem.* **2015**, *13*, 4785–4794. [[CrossRef](#)]
22. Katrun, P.; Chiampanichayakul, S.; Korworapan, K.; Pohmakotr, M.; Reutrakul, V.; Jaipetch, T.; Kuhakarn, C. PhI(OAc)₂/KI-Mediated Reaction of Aryl Sulfinates with Alkenes, Alkynes, and α,β -Unsaturated Carbonyl Compounds: Synthesis of Vinyl Sulfones and β -Iodovinyl Sulfones. *Eur. J. Org. Chem.* **2010**, *2010*, 5633–5641. [[CrossRef](#)]

23. Meesin, J.; Katrun, P.; Pareseecharoen, C.; Pohmakotr, M.; Reutrakul, V.; Soorukram, D.; Kuhakarn, C. Iodine-catalyzed Sulfonylation of Arylacetylenic Acids and Arylacetylenes with Sodium Sulfinates: Synthesis of Arylacetylenic Sulfones. *J. Org. Chem.* **2016**, *81*, 2744–2752. [CrossRef] [PubMed]
24. Meesin, J.; Katrun, P.; Reutrakul, V.; Pohmakotr, M.; Soorukram, D.; Kuhakarn, C. Decarboxylative sulfonylation of arylpropionic acids with sulfinic acids: Synthesis of (E)-vinyl sulfones. *Tetrahedron* **2016**, *72*, 1440–1446. [CrossRef]
25. Sangpheak, K.; Tabtimmai, L.; Seetaha, S.; Rungnim, C.; Chavasiri, W.; Wolschann, P.; Choowongkamon, K.; Rungrotmongkol, T. Biological Evaluation and Molecular Dynamics Simulation of Chalcone Derivatives as Epidermal Growth Factor-Tyrosine Kinase Inhibitors. *Molecules* **2019**, *24*, 1092. [CrossRef] [PubMed]
26. Daina, A.; Michielin, O.; Zoete, V. SwissADME: A free web tool to evaluate pharmacokinetics, drug-likeness and medicinal chemistry friendliness of small molecules. *Sci. Rep.* **2017**, *7*, 42717. [CrossRef]
27. Lipinski, C.A. Lead- and drug-like compounds: The rule-of-five revolution. *Drug Discov. Today Technol.* **2004**, *1*, 337–341. [CrossRef]
28. Fink, B.E.; Vite, G.D.; Mastalerz, H.; Kadow, J.F.; Kim, S.H.; Leavitt, K.J.; Du, K.; Crews, D.; Mitt, T.; Wong, T.W.; et al. New dual inhibitors of EGFR and HER2 protein tyrosine kinases. *Bioorg. Med. Chem. Lett.* **2005**, *15*, 4774–4779. [CrossRef]
29. Parganas, E.; Wang, D.; Stravopodis, D.; Topham, D.J.; Marine, J.-C.; Teglund, S.; Vanin, E.F.; Bodner, S.; Colamonici, O.R.; van Deursen, J.M.; et al. Jak2 Is Essential for Signaling through a Variety of Cytokine Receptors. *Cell* **1998**, *93*, 385–395. [CrossRef]
30. Liu, W.J.; Liu, X.J.; Xu, J.; Li, L.; Li, Y.; Zhang, S.H.; Wang, J.L.; Miao, Q.F.; Zhen, Y.S. EGFR-targeting, beta-defensin-tailored fusion protein exhibits high therapeutic efficacy against EGFR-expressed human carcinoma via mitochondria-mediated apoptosis. *Acta Pharmacol. Sin.* **2018**, *39*, 1777–1786. [CrossRef]
31. Demiray, A.; Yaren, A.; Karagenc, N.; Bir, F.; Demiray, A.; Karagur, E.; Tokgun, O.; Elmas, L.; Akca, H. The Frequency of EGFR and KRAS Mutations in the Turkish Population with Non-small Cell Lung Cancer and their Response to Erlotinib Therapy. *Balk. J. Med. Genet.* **2018**, *21*, 21–26. [CrossRef]
32. Hirano, T.; Yasuda, H.; Tani, T.; Hamamoto, J.; Oashi, A.; Ishioka, K.; Arai, D.; Nukaga, S.; Miyawaki, M.; Kawada, I.; et al. In vitro modeling to determine mutation specificity of EGFR tyrosine kinase inhibitors against clinically relevant EGFR mutants in non-small-cell lung cancer. *Oncotarget* **2015**, *6*, 38789–38803. [CrossRef]
33. Li, Y.; Song, Z.; Jin, Y.; Tang, Z.; Kang, J.; Ma, X. Novel Selective and Potent EGFR Inhibitor that Overcomes T790M-Mediated Resistance in Non-Small Cell Lung Cancer. *Molecules* **2016**, *21*, 1462. [CrossRef]
34. Sharma, V.K.; Nandekar, P.P.; Sangamwar, A.; Pérez-Sánchez, H.; Agarwal, S.M. Structure guided design and binding analysis of EGFR inhibiting analogues of erlotinib and AEE788 using ensemble docking, molecular dynamics and MM-GBSA. *RSC Adv.* **2016**, *6*, 65725–65735. [CrossRef]
35. Liu, B.; Bernard, B.; Wu, J.H. Impact of EGFR point mutations on the sensitivity to gefitinib: Insights from comparative structural analyses and molecular dynamics simulations. *Proteins* **2006**, *65*, 331–346. [CrossRef]
36. Doss, G.P.; Rajith, B.; Chakraborty, C.; NagaSundaram, N.; Ali, S.K.; Zhu, H. Structural signature of the G719S-T790M double mutation in the EGFR kinase domain and its response to inhibitors. *Sci. Rep.* **2014**, *4*, 5868. [CrossRef]
37. Martinez-Jimenez, F.; Overington, J.P.; Al-Lazikani, B.; Marti-Renom, M.A. Rational design of non-resistant targeted cancer therapies. *Sci. Rep.* **2017**, *7*, 46632. [CrossRef]
38. Stamos, J.; Sliwkowski, M.X.; Eigenbrot, C. Structure of the epidermal growth factor receptor kinase domain alone and in complex with a 4-anilinoquinazoline inhibitor. *J. Biol. Chem.* **2002**, *277*, 46265–46272. [CrossRef]
39. Ahmed, M.; Sadek, M.M.; Abouzid, K.A.; Wang, F. In silico design: Extended molecular dynamic simulations of a new series of dually acting inhibitors against EGFR and HER2. *J. Mol. Graph. Model.* **2013**, *44*, 220–231. [CrossRef]
40. Cheng, H.C. The power issue: Determination of KB or Ki from IC50: A closer look at the Cheng–Prusoff equation, the Schild plot and related power equations. *J. Pharmacol. Toxicol. Methods* **2001**, *46*, 61–71. [CrossRef]
41. Mahalapbutr, P.; Thitinanthavet, K.; Kedkham, T.; Nguyen, H.; Theu, L.; Dokmaisrijan, S.; Huynh, L.; Kungwan, N.; Rungrotmongkol, T. A theoretical study on the molecular encapsulation of luteolin and pinocembrin with various derivatized beta-cyclodextrins. *J. Mol. Struct.* **2019**, *1180*, 480–490. [CrossRef]
42. Kammarabutr, J.; Mahalapbutr, P.; Nutho, B.; Kungwan, N.; Rungrotmongkol, T. Low susceptibility of asunaprevir towards R155K and D168A point mutations in HCV NS3/4A protease: A molecular dynamics simulation. *J. Mol. Graph. Model.* **2019**, *89*, 122–130. [CrossRef]
43. Sanachai, K.; Mahalapbutr, P.; Choowongkamon, K.; Poo-Arporn, R.P.; Wolschann, P.; Rungrotmongkol, T. Insights into the Binding Recognition and Susceptibility of Tofacitinib toward Janus Kinases. *ACS Omega* **2020**, *5*, 369–377. [CrossRef]
44. Marvin Was Used for Drawing, Displaying and Characterizing Chemical Structures, Substructures and Reactions, Marvin 17.21.0, ChemAxon. Available online: <https://www.chemaxon.com> (accessed on 19 June 2020).
45. Pettersen, E.F.; Goddard, T.D.; Huang, C.C.; Couch, G.S.; Greenblatt, D.M.; Meng, E.C.; Ferrin, T.E. UCSF chimera-A visualization system for exploratory research and analysis. *J. Comput. Chem.* **2004**, *25*, 1605–1612. [CrossRef]
46. Cheng, F.; Li, W.; Zhou, Y.; Shen, J.; Wu, Z.; Liu, G.; Lee, P.W.; Tang, Y. admetSAR: A Comprehensive Source and Free Tool for Assessment of Chemical ADMET Properties. *J. Chem. Inf. Model.* **2012**, *52*, 3099–3105. [CrossRef]
47. Seetaha, S.; Ratanabunyong, S.; Choowongkamon, K. Expression, purification, and characterization of the native intracellular domain of human epidermal growth factor receptors 1 and 2 in Escherichia coli. *Appl. Microbiol. Biotechnol.* **2019**, *103*. [CrossRef]

48. Mahalapbutr, P.; Wonganan, P.; Charoenwongpaiboon, T.; Prousoontorn, M.; Chavasiri, W.; Rungrotmongkol, T. Enhanced Solubility and Anticancer Potential of Mansonone G By beta-Cyclodextrin-Based Host-Guest Complexation: A Computational and Experimental Study. *Biomolecules* **2019**, *9*, 545. [[CrossRef](#)]
49. Mahalapbutr, P.; Nutho, B.; Wolschann, P.; Chavasiri, W.; Kungwan, N.; Rungrotmongkol, T. Molecular insights into inclusion complexes of mansonone E and H enantiomers with various beta-cyclodextrins. *J. Mol. Graph. Model.* **2018**, *79*, 72–80. [[CrossRef](#)]
50. Phanich, J.; Rungrotmongkol, T.; Kungwan, N.; Hannongbua, S. Role of R292K mutation in influenza H7N9 neuraminidase toward oseltamivir susceptibility: MD and MM/PB(GB)SA study. *J. Comput. Aided Mol. Des.* **2016**, *30*, 917–926. [[CrossRef](#)]
51. Maier, J.A.; Martinez, C.; Kasavajhala, K.; Wickstrom, L.; Hauser, K.E.; Simmerling, C. ff14SB: Improving the Accuracy of Protein Side Chain and Backbone Parameters from ff99SB. *J. Chem. Theory Comput.* **2015**, *11*, 3696–3713. [[CrossRef](#)]
52. Sangpheak, W.; Khuntawee, W.; Wolschann, P.; Pongsawasdi, P.; Rungrotmongkol, T. Enhanced stability of a naringenin/2,6-dimethyl beta-cyclodextrin inclusion complex: Molecular dynamics and free energy calculations based on MM- and QM-PBSA/GBSA. *J. Mol. Graph. Model.* **2014**, *50*, 10–15. [[CrossRef](#)] [[PubMed](#)]
53. Jorgensen, W.L.; Chandrasekhar, J.; Madura, J.D.; Impey, R.W.; Klein, M.L. Comparison of simple potential functions for simulating liquid water. *J. Chem. Phys.* **1983**, *79*, 926–935. [[CrossRef](#)]
54. Chari, R.; Jerath, K.; Badkar, A.V.; Kalonia, D.S. Long- and short-range electrostatic interactions affect the rheology of highly concentrated antibody solutions. *Pharm. Res.* **2009**, *26*, 2607–2618. [[CrossRef](#)] [[PubMed](#)]
55. York, D.M.; Darden, T.A.; Pedersen, L.G. The effect of long-range electrostatic interactions in simulations of macromolecular crystals: A comparison of the Ewald and truncated list methods. *J. Chem. Phys.* **1993**, *99*, 8345–8348. [[CrossRef](#)]
56. Ryckaert, J.-P.; Ciccotti, G.; Berendsen, H.J.C. Numerical integration of the cartesian equations of motion of a system with constraints: Molecular dynamics of n-alkanes. *J. Comput. Phys.* **1977**, *23*, 327–341. [[CrossRef](#)]
57. Roe, D.R.; Cheatham, T.E., III. PTRAJ and CPPTRAJ: Software for Processing and Analysis of Molecular Dynamics Trajectory Data. *J. Chem. Theory Comput.* **2013**, *9*, 3084–3095. [[CrossRef](#)]
58. Genheden, S.; Ryde, U. The MM/PBSA and MM/GBSA methods to estimate ligand-binding affinities. *Expert Opin. Drug Discov.* **2015**, *10*, 449–461. [[CrossRef](#)]
59. Sulea, T.; Cui, Q.; Purisima, E.O. Solvated Interaction Energy (SIE) for Scoring Protein–Ligand Binding Affinities. 2. Benchmark in the CSAR-2010 Scoring Exercise. *J. Chem. Inf. Model.* **2011**, *51*, 2066–2081. [[CrossRef](#)]